Engineering Structures 330 (2025) 119904

Contents lists available at ScienceDirect

Engineering Structures

journal homepage: www.elsevier.com/locate/engstruct

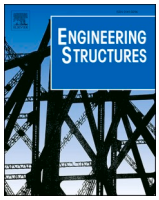

A hybrid domain adaptation approach for estimation of prestressed forces in prestressed concrete bridges under moving vehicles

Saeid Talaei [a,*], Xinqun Zhu [a,*], Jianchun Li [a], Yang Yu [b], Tommy H.T. Chan [c]

[a] School of Civil and Environmental Engineering, University of Technology Sydney, Ultimo, NSW 2007, Australia
[b] Centre for Infrastructure Engineering and Safety, School of Civil and Environmental Engineering, The University of New South Wales, Sydney, NSW 2052, Australia
[c] School of Civil and Environmental Engineering, The Queensland University of Technology (QUT), Brisbane, QLD 2052, Australia

ARTICLE INFO

Keywords:
Prestress force estimation
Vehicle-bridge interaction
Continuous wavelet transform
Hybrid domain adaptation

ABSTRACT

Ensuring the accurate and reliable estimation of prestressed forces (PFs) in prestressed concrete bridges is vital for operational performance and public safety. Traditional vibration-based methods often face challenges when applied to real-world scenarios. In this study, a novel hybrid domain adaptation approach is proposed to predict the prestressed force of prestressed concrete bridges under moving vehicles. The finite element model for Vehicle-Bridge Interaction (VBI) systems is established and validated using the experimental results. This validated model is then used to generate a synthetic training dataset of the source domain. Continuous Wavelet Transform (CWT) is employed for feature extraction from VBI acceleration responses, capturing their time-frequency properties. Preliminary feature extraction is enhanced through the use of a pre-trained AlexNet network. Following this initial step, a novel hybrid domain adaptation (DA) approach is applied to close the gap between the synthetic and real-world data. Specifically, Maximum Mean Discrepancy (MMD) and adversarial DA techniques are synergistically combined. Three types of loss functions are incorporated: Regression Loss for precise force prediction, MMD Loss to align the synthetic and real-world data domains, and Adversarial Loss to ensure domain invariance. The effects of uncertainties in VBI system, such as errors of the bridge length, flexural rigidity, density, damping, boundary conditions, errors of the vehicle model and moving speed and road surface roughness, have been discussed. The results indicate that the integrated approach effectively mitigates the challenges posed by domain shift, enabling robust and reliable predictions of PFs in actual bridge structures. The finding of this study offers a comprehensive, data-driven solution with significant implications for the future of structural health monitoring and bridge condition assessment.

1. Introduction

Bridges are essential components of urban infrastructure, enabling the continuous flow of economic activities. Prestressed concrete (PSC) bridges, which utilise compressive stresses to counteract tensile stresses, represent a significant advancement in bridge technology [13]. This prestressing technique increases bridges' service load capacity, controls crack formation, and reduces deflection, making PSC bridges both efficient and cost-effective [36]. However, the prestress force is expected to reduce over time due to factors such as creep and shrinkage of concrete, relaxation of steel, frictional loss, and corrosion. Excessive reduction in the prestress force can severely impair a bridge's structural integrity and safety [14]. Therefore, it is crucial to monitor the prestress force in PCB bridges to ensure that it remains within a safe range.

The development of non-destructive methods for estimating the prestressed force in PSC bridges has attracted the interest of researchers and engineers. Traditional local non-destructive techniques are time-consuming and costly and require special equipment [5]. Vibration-based methods, on the other hand, have been developed and used to predict the prestress loss through changes in structural dynamic responses. Yi et al. [37] presented a clustering number determination for output-only modal identification. Chan and Yung [7] presented that natural frequencies of PCB bridges reduce with the increase of prestress forces by the compression softening effect. Breccolotti [6] stated that an increase in prestressing leads to a rise in natural frequencies at low prestressing force levels. However, as the prestressing force intensifies, the growth rate of the natural frequency decreases. Thedy et al. [32] also verified that the vibrational frequencies of internally prestressed

* Corresponding authors.
E-mail addresses: saeid.talaei@student.uts.edu.au (S. Talaei), xinqun.zhu@uts.edu.au (X. Zhu).

https://doi.org/10.1016/j.engstruct.2025.119904
Received 1 September 2024; Received in revised form 3 February 2025; Accepted 6 February 2025
Available online 19 February 2025
0141-0296/© 2025 The Author(s). Published by Elsevier Ltd. This is an open access article under the CC BY license (http://creativecommons.org/licenses/by/4.0/).

concrete beams are significantly influenced by the profile of the tendon and boundary conditions. Wu et al. [34] presented a method for damage detection of tension pendulums using structural frequency variance. As noted above, variations in prestress force do not have a significant effect on the dynamic behaviour of PC bridges [4], and the natural frequency is insensitive or uncertain to the change of the prestress force in PSB bridges.

Recently, the forced vibration responses have been used to estimate the prestress force through inverse calculations. Lu and Law [22] utilised time-domain responses of the beam subjected to both sinusoidal and impact forces to estimate the prestressed force in a PSC girder, utilising the orthogonal polynomial function and Tikhonov regularisation techniques to mitigate noise effects. Other approaches that leverage the vehicle bridge interactive (VBI) responses are highly valued in bridge condition monitoring, as moving vehicles are the primary live load on bridge structures [38]. Law et al. [17] introduced a wavelet-based method to identify changes in prestressing forces with wavelet techniques to identify moving forces and prestress in bridge-vehicle systems simultaneously. Li et al. [20] utilised VBI responses to identify the elemental prestress force. Dynamic response sensitivity-based finite element model updating was proposed to identify the prestress force, but a large error was observed due to the rough road conditions. Xiang et al. [35] proposed a method to identify moving load and prestressed force of a simply supported prestressed concrete beam. Their method involved transforming the prestressed force into an external pseudo-load localised in each beam element using the Virtual Distortion Method (VDM). Utilising dynamic responses of a bridge under moving vehicles for prestressed force identification offers advantages. The identification is conducted under operational conditions, yielding more reliable and accurate results for real-world applications. Moreover, compared to conventional bridge monitoring systems, the number of required sensors can be reduced significantly. However, the accuracy of these methods depends on the precision of the VBI model. Factors such as road surface roughness, modelling errors, the wheel-bridge contact model, and measurement noise induce uncertainties, affecting identification results [30].

Data-driven methods, utilising the power of machine learning (ML) algorithms, present a promising avenue to address these challenges. These methods can process vast amounts of high-dimensional data to evaluate bridge conditions [1]. While traditional ML techniques are heavily reliant on feature extraction, deep learning (DL) methods, like convolutional neural networks (CNNs), can autonomously extract optimal features from raw data, enhancing identification performance [2]. Yang and Huang [36] adopted CNNs, to identify damages in prestressed concrete beam bridges. Their method combines the flexibility curvature and CNN to predict the damage location and extent of prestressed concrete beams. Nguyen et al. [24] proposed an impedance-based damage detection method using deep learning. A one-dimensional CNN model is used to extract the optimal PF-sensitive features from raw impedance signals. However, the effective training of DL networks necessitates a considerable volume of high-quality labelled data corresponding to different damage states of the structure for training, which is not feasible to obtain from a real bridge structure [2]. Still, a DL can be trained using a dataset built by an updated finite element model. The updated FE model needs to imitate the structural behaviour impeccably. Model updating techniques can be employed to reduce the gap between the FE model and the real structure. However, the modelling errors can never be completely eliminated, and the results of health/condition monitoring are always dependent on the performance of the updated model.

Transfer learning methods can be effectively used to overcome this issue by transferring the knowledge learnt from a FE model to the real-world structure without needing a low-level model updating [10]. Transfer learning methods, such as Domain Adaptation (DA), can minimize the domain shift between the finite element model and the real structure. The core idea behind DA is to leverage the knowledge from a source domain, where abundant labelled data is available, to improve the learning performance in a target domain with limited labelled data [8]. One of the prominent approaches in DA is the Maximum Mean Discrepancy (MMD) method, which aims to minimize the distribution discrepancy between the source and target domains by matching their feature means in a Reproducing Kernel Hilbert Space (RKHS) [16]. However, the application of DA in structural condition monitoring is limited so far. Gardner et al. [10] utilised joint domain adaptation (JDA) to bridge the gap between the FE model and an experimental setup of a three-story building. They used the first three natural frequencies as damage-sensitive features and demonstrated that their approach could effectively label unknown damage states in a real structure. However, their study assumed that the same damage classes were available in both the source and target domains, which is not often the case in real-world applications. Poole et al. [27] introduced a partial DA framework that accounts for class imbalance between the source and target domains. Their approach also utilised natural frequencies as features and is more realistic as it assumes that not all damage scenarios are labelled in the target domain. However, their method has a significant drawback, i.e. it requires time-consuming pre-processing every time a new condition appears in the structure, unsuitable for real-time monitoring.

In this study, a novel hybrid DA approach is proposed for predicting PFs in prestressed concrete bridges. Recognizing the inherent challenges of limited labelled data in real-world scenarios, a finite element model is established to generate a comprehensive synthetic training dataset as a source domain. This dataset, while rich in information, contains domain discrepancies when compared to real-world data from fully prestressed bridges. To address this issue, MMD and adversarial DA are integrated in the proposed approach. Alignment of features extracted from synthetic and real-world data is achieved using MMD, and domain-invariance is ensured through adversarial learning. This results in a unified feature space suitable for accurate prediction. By integrating VBI analysis, time-frequency representation of acceleration data, feature extraction using a pre-trained AlexNet network, and hybrid DA strategies, this study aims to offer a comprehensive, data-driven solution with significant implications for the future of structural health monitoring and bridge condition assessment. The results indicate that this approach not only mitigates the challenges posed by domain shift but also paves the way for robust and reliable predictions of PFs in real-world bridge structures.

2. Methodology

To keep knowledge integrity, the introduction of fundamental concepts of the proposed method is detailed in this section. The overall workflow of the proposed methodology is provided in Fig. 1.

2.1. Vehicle-bridge interaction (VBI) analysis

A typical VBI system is depicted in Fig. 2. A simply supported bridge with a uniform cross-section is subjected to a two-axle vehicle moving at a constant speed V. The vehicle is a system with four degrees of freedom. It is assumed that the vehicle keeps in contact with the bridge during its passage. The VBI system includes the vehicle and bridge sub-systems.

The bridge is modelled by N beam elements. The equations of motion for vehicle and bridge models are obtained as:

$$\text{Bridge}: \boldsymbol{M}_b\ddot{\boldsymbol{d}}_b + \boldsymbol{C}_b\dot{\boldsymbol{d}}_b + \overline{\boldsymbol{K}}_b\boldsymbol{d}_b = \boldsymbol{\phi}(t)\boldsymbol{P}_{bint}(t) \tag{1}$$

$$\text{Vehicle}: \boldsymbol{M}_v\ddot{\boldsymbol{d}}_v + \boldsymbol{C}_v\dot{\boldsymbol{d}}_v + \boldsymbol{K}_v\boldsymbol{d}_v = \boldsymbol{P}_{vint}(t) \tag{2}$$

where $\ddot{\boldsymbol{d}}_b$, $\dot{\boldsymbol{d}}_b$, $\boldsymbol{d}_b$ are nodal acceleration, velocity, and displacement vectors of the bridge, respectively. $\boldsymbol{M}_b$, $\boldsymbol{C}_b$ and $\overline{\boldsymbol{K}}_b$ denote the mass, damping, and stiffness matrices of the prestressed bridge, respectively. $\boldsymbol{P}_{bint}(t)$ is the force acting on the bridge by the vehicle. $\boldsymbol{P}_{vint}(t)$ is the interaction force to the vehicle. α and β are the constants of Rayleigh damping.

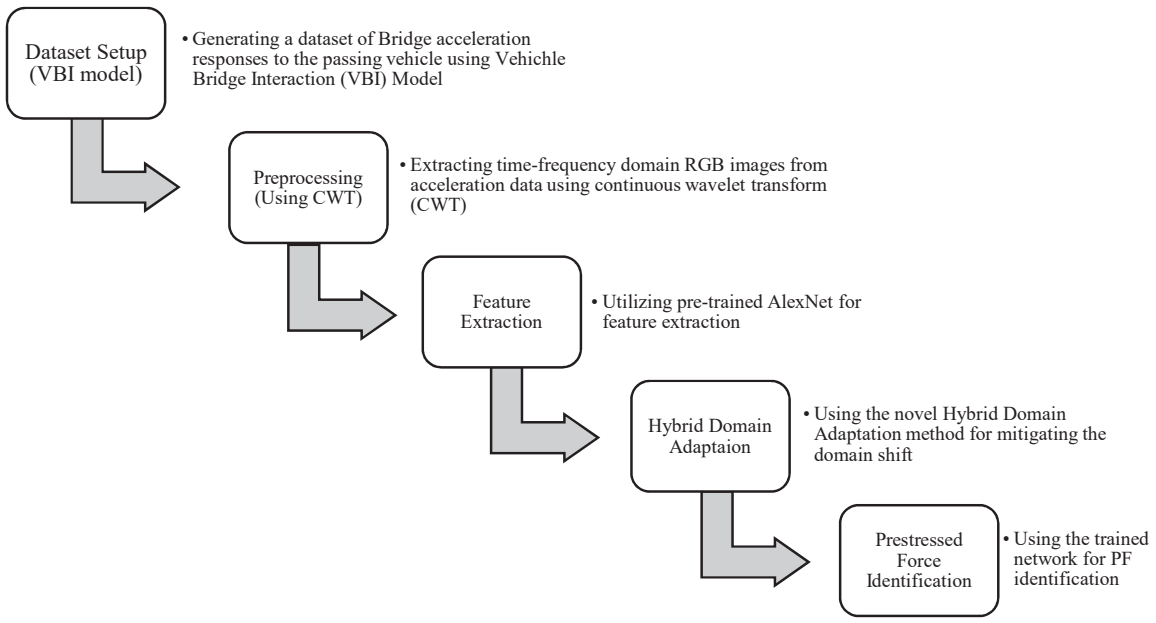

Fig. 1. Overall methodology of the proposed approach.

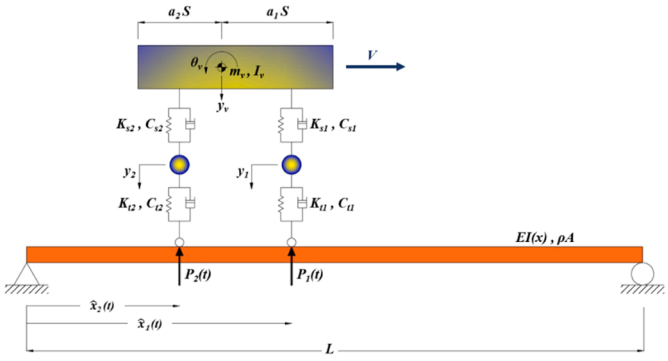

Fig. 2. The VBI model.

$$\boldsymbol{C}_b = \alpha \mathbf{M}_b + \beta \mathbf{K}_b \tag{3}$$

$$\overline{\boldsymbol{K}}_b = \boldsymbol{K}_b - \boldsymbol{K}_{Gb} \tag{4}$$

where $\boldsymbol{K}_b$ is the global stiffness matrix without PF. $\boldsymbol{K}_{Gb}$ is additional stiffness matrix due to the prestressing effect, which can be written as:

$$\boldsymbol{K}_{Gb} = \frac{P_0}{l_e}\begin{bmatrix} \frac{6}{5} & \frac{l_e}{10} & -\frac{6}{5} & \frac{l_e}{10} \\ \frac{l_e}{10} & \frac{2l_e^2}{15} & -\frac{l_e}{10} & -\frac{l_e^2}{30} \\ -\frac{6}{5} & -\frac{l_e}{10} & \frac{6}{5} & -\frac{l_e}{10} \\ \frac{l_e}{10} & -\frac{l_e^2}{30} & -\frac{l_e}{10} & \frac{2l_e^2}{15} \end{bmatrix} \tag{5}$$

where P_0 is the PF and l_e is the element length. $\boldsymbol{K}_v$, $\boldsymbol{C}_v$ and $\boldsymbol{M}_v$ are the stiffness, damping and mass matrices of the vehicle, respectively. $\ddot{\boldsymbol{d}}_v$, $\dot{\boldsymbol{d}}_v$, $\boldsymbol{d}_v$ are the acceleration, velocity and displacement responses of the vehicle respectively where $\boldsymbol{d}_v = \{y_v, \theta_v, y_1, y_2\}^T$. As shown in Fig. 2, y_v, θ_v, y_1, y_2 are the vertical displacement and rotation of the vehicle body, and the vertical displacements of the front and rear axles respectively.

$$\mathbf{M}_V = \begin{bmatrix} m_v & 0 & 0 & 0 \\ 0 & I_v & 0 & 0 \\ 0 & 0 & m_1 & 0 \\ 0 & 0 & 0 & m_2 \end{bmatrix} \tag{6}$$

$$\mathbf{C}_V = \begin{bmatrix} C_{s1} + C_{s2} & -C_{s1}a_1 + C_{s2}a_2' & -C_{s1} & -C_{s2} \\ (-C_{s1}a_1 + C_{s2}a_2)S & (C_{s1}a_1^2 + C_{s2}a_2^2)S & C_{s1}a_1 S & -C_{s2}a_2 S \\ -C_{s1} & C_{s1}a_1 S & C_{s1} & 0 \\ -C_{s2} & -C_{s2}a_2 S & 0 & C_{s2} \end{bmatrix} \tag{7}$$

$$\mathbf{K}_V = \begin{bmatrix} K_{s1} + K_{s2} & (-K_{s1}a_1 + K_{s2}a_2)S & -K_{s1} & -K_{s2} \\ (-K_{s1}a_1 + K_{s2}a_2)S & (K_{s1}a_1^2 + K_{s2}a_2^2)S^2 & K_{s1}a_1 S & -K_{s2}a_2 S \\ -K_{s1} & K_{s1}a_1 S & K_{s1} & 0 \\ -K_{s2} & -K_{s2}a_2 S & 0 & K_{s2} \end{bmatrix} \tag{8}$$

To simplify the expression for multiple interaction forces (e.g. vehicle with multiple axles), $\boldsymbol{P}_{bint}(t)$ is expressed as $\boldsymbol{P}(t) = \{P_1(t), P_2(t), \ldots, P_l(t), \ldots, P_{N_p}(t)\}^T$ where N_p is the number of interaction forces as depicted in Fig. 2. A time-dependent factor is defined as $\boldsymbol{\phi}(t)$ to incorporate the time-variant nature of the moving forces. $\boldsymbol{\phi}(t) = \{\boldsymbol{\phi}_1, \boldsymbol{\phi}_2 \ldots \boldsymbol{\phi}_l \ldots \boldsymbol{\phi}_{N_p}\}$ is a $2(N+1)\times N_p$ matrix, while $\boldsymbol{\phi}_l = \{000 \ldots \boldsymbol{\psi}_i \ldots 000\}^T$ and $\boldsymbol{\psi}_i$ is the vector of shape functions for the force $P_l(t)$, located on $\hat{x}_l(t)$ [19].

$$\boldsymbol{\psi}_i = \begin{Bmatrix} 1 - 3X + 2X^3 \\ Xl_e(X-1)^2 \\ 3X^2 - 2X^3 \\ X^2 l_e(X-1) \end{Bmatrix}^T, X = \left[\frac{\hat{x}_l(t) - (i-1)l_e}{l_e}\right] \quad , (i-1)l_e \leqslant \hat{x}_l(t) < (i)l_e \tag{9}$$

Combining Eqs. (1) and (2), the equation of motion for the VBI system can be expressed as:

$$\begin{bmatrix} \boldsymbol{M}_b & \boldsymbol{M}_v\boldsymbol{\phi} \\ 0 & \boldsymbol{M}_v \end{bmatrix} \begin{bmatrix} \ddot{\boldsymbol{d}}_b \\ \ddot{\boldsymbol{d}}_v \end{bmatrix} + \begin{bmatrix} \boldsymbol{C}_b & 0 \\ -\boldsymbol{C}_v\boldsymbol{\phi}^T & \boldsymbol{C}_v \end{bmatrix} \begin{bmatrix} \dot{\boldsymbol{d}}_b \\ \dot{\boldsymbol{d}}_v \end{bmatrix} + \begin{bmatrix} \boldsymbol{K}_b & 0 \\ -\boldsymbol{K}_v\boldsymbol{\phi}^T - \boldsymbol{C}_v\dot{\boldsymbol{\phi}}^T & \boldsymbol{K}_v \end{bmatrix} \begin{bmatrix} \boldsymbol{d}_b \\ \boldsymbol{d}_v \end{bmatrix} = \begin{bmatrix} \boldsymbol{\phi}\boldsymbol{M}_v\boldsymbol{g} \\ \boldsymbol{K}_v r(x) + \boldsymbol{C}_v r'(x) V \end{bmatrix} \tag{10}$$

where $r(x)$ is road surface roughness and V is the vehicle speed. According to ISO 8608 specification [25], the power spectral density function $S_{rr}(\omega)$ of the road roughness is as below:

$$\begin{cases} S_{rr}(\omega) = S_{rr}(\omega_0)(\omega/\omega_0)^{-2} (\omega \leqslant \omega_0) \\ S_{rr}(\omega) = S_{rr}(\omega_0)(\omega/\omega_0)^{-1.5} (\omega > \omega_0) \end{cases} \tag{11}$$

where ω is the angular frequency. ω_0 stands for the standard frequency equal to $0.16 \times V$ Hz. $S_{rr}(\omega_0)$ is the amplitude of power spectral density function at the standard frequency [31]. The road surface roughness is obtained by the inverse Fourier transform on $S_{rr}(\omega)$.

2.2. Time-frequency analysis

The responses of the VBI system can be obtained by solving Eq. (10). While the time-domain representation obscures frequency details and the frequency-domain overlooks time variations, the time-frequency analysis could capture the information in both time and frequency domains. In this study, the continuous wavelet transform (CWT) is used. Unlike the short-time Fourier transform, which uses fixed sinusoid functions, CWT employs scalable and translatable wavelet functions to analyse the signal. This makes CWT particularly effective for non-stationary signals. The time-frequency representation by CWT can be visualized as an image, capturing the energy distribution over time and frequency. These images are utilised as the input for machine learning (ML) models [29]. The image represents the energy distribution of the signal in the time and frequency domain. The CWT of a VBI response signal $x(t)$ is obtained as:

$$CWT(a,b) = \frac{1}{\sqrt{a}} \int x(t)\mu\left(\frac{t-b}{a}\right) dt \tag{12}$$

where b is the translation parameter, and a is the scale parameter to determine the size of the wavelet function [3]. $\mu(t)$ is the wavelet function as:

$$\mu(t) = \pi^{-1/4} \; e^{i\omega_0 t} \; e^{-t^2/2} \tag{13}$$

where ω_0 is set to 6, which is the centre frequency of the wavelet function. Fig. 3 depicts the time-frequency representation of the VBI response alongside its time and frequency domain counterparts. The CWT representation captures the local time-varying characteristics of the VBI system when the vehicle is passing over the bridge.

2.3. Validation of the VBI model

Compared with the previous VBI model [18], the proposed VBI model includes the prestress effect, and the new model is used to generate the simulation data for prestress force estimation using the hybrid domain adaptation-based method. The experimental validation of the proposed VBI model was conducted based on existing experimental data by Law and Zhu [18]. This involved a reinforced concrete beam with a Tee-section, measuring five meters in length, across which a vehicle was towed at a speed of roughly 0.5 m/s using an electric motor. The vehicles used in the experiment varied in weight, with the lighter one weighing 1081.6 kg and the heavier one 1536.7 kg. Wheel damping and stiffness values were established at 8.94×10^3 N/(m/s) and 6.23×10^6 N/m, respectively. The beam's rigidity (EI) was determined to be 5.59×10^7 N.m^2 based on its cross-sectional properties. Further details on the experimental arrangement are provided in the work of Law and Zhu [18]. In this study, the experimental results were used to validate the fundamental VBI model assumptions and the accuracy of

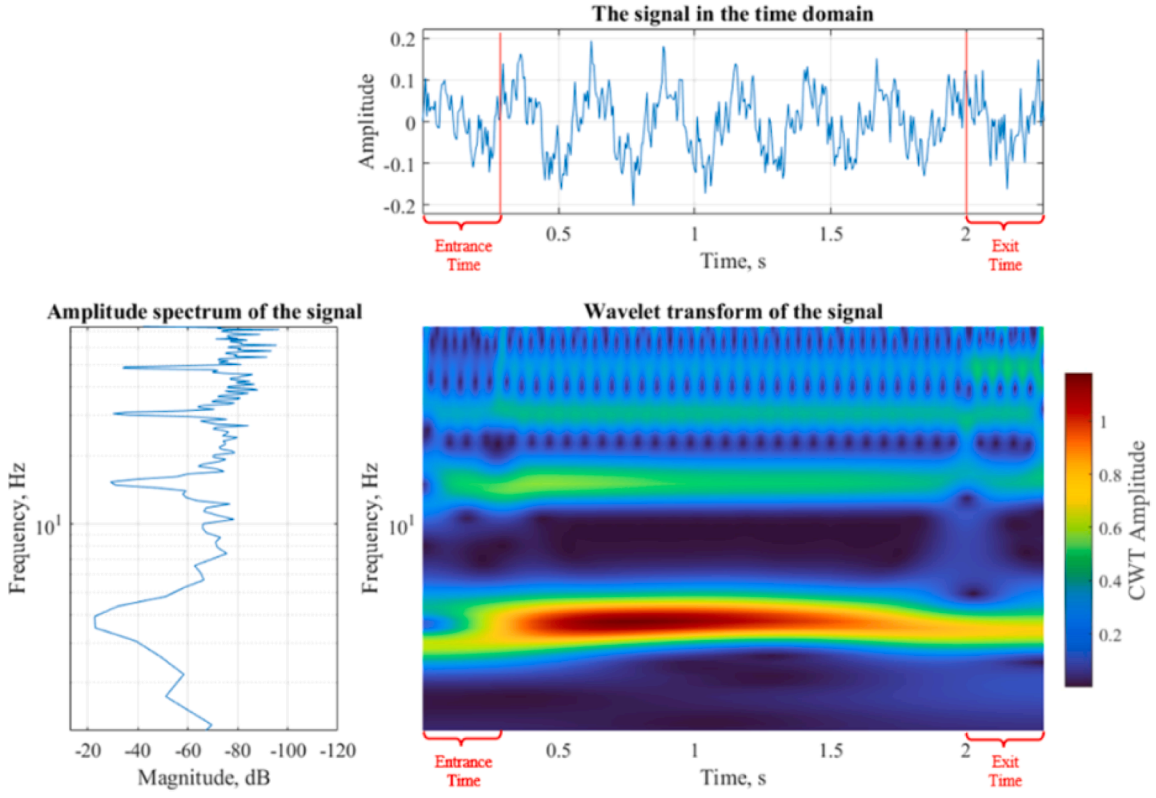

Fig. 3. Representation of the VBI acceleration response of the bridge at 3/8 span of the beam in time, frequency, and time-frequency domains (Talaei et al., 2023).

the VBI model was not critical for the proposed hybrid domain adaptation framework. The displacement responses were compared. Fig. 4 presents a comparative analysis of the experimental and numerical results for displacements at the 3/8 span under the influence of both vehicle weights. This comparison underscores the precision and reliability of the numerical model in generating the responses of the bridge subjected to a moving vehicle.

In this study, the validated numerical model is used to generate the VBI response data. Fig. 5 shows the time-frequency spectrum of VBI responses for three levels of PF. From the results, it is evident that the time-frequency representation varies with the PF.

3. DL-basED PF-sensitive feature extraction

In this section, a DL-based PF-sensitive feature extraction method is proposed and numerically validated. Firstly, the VBI model is utilised to generate the acceleration responses of the bridge with a range of prestressed forces. Secondly, CWT is applied to represent the acceleration data in the time-frequency domain and form the 2D-images corresponding to each PF label. This is followed by utilising a pre-trained AlexNet network for feature extraction.

3.1. Nominated VBI model for data generation

In this study, a two-axle vehicle passing the bridge is adopted to analyze the VBI system. The length of the bridge is 30 m. The parameters of the bridge model are the flexural rigidity of 2.5×10^{10} N·m^2, the mass per unit length of 5000 kg/m and the prestress force ranging from 0 to 10×10^6 N. The parameters of the vehicle are as [23]: the mass of vehicle, front and rear wheels are $m_v = 17735kg$, $m_1 = 1500kg$, $m_2 = 1000kg$ respectively; the pitching inertia of the vehicle body is $I_v = 1.47 \times 10^5 kg \bullet m^2$; the stiffness and damping coefficients of the suspension system for the front and rear axles are $K_{s1} = 2.47 \times 10^6 N/m$ and $C_{s1} = 3.00 \times 10^4 Nm/s$, and $K_{s2} = 4.23 \times 10^6 N/m$ and $C_{s2} = 4.00 \times 10^4 Nm/s$ respectively; the stiffness and damping coefficients of the front and rear wheels are $K_{t1} = 3.74 \times 10^6 N/m$; $K_{t2} = 4.60 \times 10^6 N/m$, and $C_{t1} = 3.90 \times 10^3 Nm/s$, $C_{t2} = 4.30 \times 10^3 Nm/s$ respectively. The axle spacing and the corresponding parameters are S= 4.27 m, and $a_1 = 0.519$, $a_2 = 0.481$ respectively.

In this study, VBI analysis is conducted with a time step of 0.001 s. The vehicle is set to move at a speed of 15 m/s, and the road surface roughness is categorized under Class A. For each level of PF, 20 samples are generated with a Signal to Noise Ratio (SNR) of 55 (50 for targets).

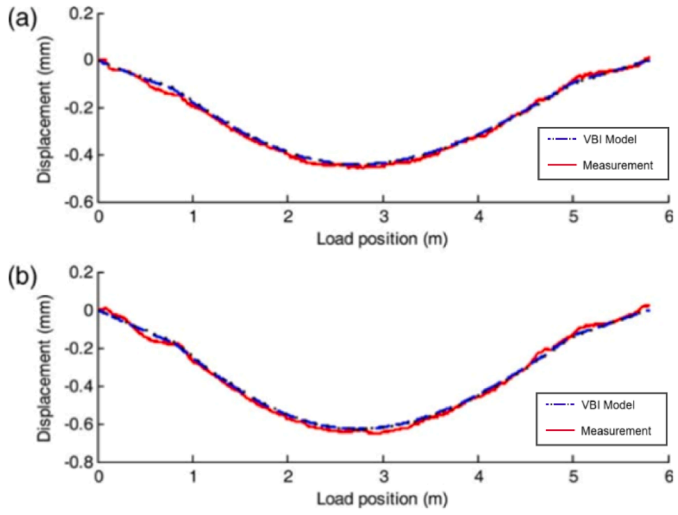

Fig. 4. Displacements at 3/8 span of the beam under different moving loads. (a) Light loads; (b) heavy loads [18].

The PF is labelled in percentages, ranging from 0 % to 100 % (10,000 KN), with increments of 5 %. These settings aim to create a synthetic dataset for training a regression model.

3.2. Feature extraction using pre-trained alex-net network

In this study, the time-frequency representation of the acceleration responses captured by three distinct sensors located on the bridge span is obtained by CWT. These three sensors are located at 3/10 L, 4/10 L, and 5/10 L of the bridge span, respectively.

For each sensor location, the CWT of the measured acceleration response produces a single-band grayscale image representing the signal's time-frequency characteristics. Three individual single-band images are obtained by performing the same procedure at three distinct sensor positions (3/10 L, 4/10 L, and 5/10 L of the bridge span). These grayscale images are subsequently merged along their channel dimension, forming a composite three-band image analogous to an RGB format. As illustrated in Fig. 6, This multi-channel representation integrates time-frequency information from three sensors, providing a more comprehensive input for subsequent feature extraction using AlexNet.

AlexNet, introduced in 2012 by Alex Krizhevsky, Ilya Sutskever, and Geoffrey Hinton, marked a groundbreaking shift in the field of deep learning [15]. It was among the earliest convolutional neural networks to successfully incorporate ReLU activations and Dropout to improve training stability and prevent overfitting. Notably, AlexNet was the first CNN-based model to achieve a winning performance in the ImageNet Large Scale Visual Recognition Challenge (ILSVRC), heralding a new era in image recognition tasks.

The selection of AlexNet over other known pre-trained networks, such as VGG16 and ResNet-50, is based on its high performance in feature extraction from CWT images of the VBI model [30]. Notably, integrating data from multiple sensors into a 3-band coloured image enriches the dataset by combining various sensor readings into a unified, informative representation. Additionally, this approach enables optimal utilisation of the pre-trained AlexNet architecture, which is inherently designed to process colored images.

3.3. Performance of the AlexNet for predicting PF

Fig. 7 shows the flowchart to evaluate the performance of the AlexNet model for predicting PFs. As shown in Fig. 7, the acceleration responses at three measurement locations of the bridge subjected to a moving vehicle are utilised to obtain the time-frequency representation by CWT, and then they are combined to form the image as the input of the AlexNet. The features extracted by the pre-trained AlexNet are used to predict the PF using a support vector regression (SVR). Fig. 8(a) shows the first three principal components of the extracted features and the correlation between the features and PFs. As shown in Fig. 8(a), there is a continuous and gradual relationship between the feature vector extracted from the AlexNet network and PF. By adding a regression layer, the output of the network model is to predict the PF. The results in Fig. 8(b) show that the predicted prestress force agrees well with the true value.

As mentioned above, both the training and testing datasets are generated using the numerical model. There is no domain discrepancy, and this is not the case in practice. In practice, the training dataset is generated using the FE model but the test data are measured from the real bridge structure. The testing data may have significant discrepancies from the training dataset due to the effect of the operational environment. This domain shift will significantly affect the performance of the AlexNet model. To overcome this issue, a novel DA method is introduced in the next section.

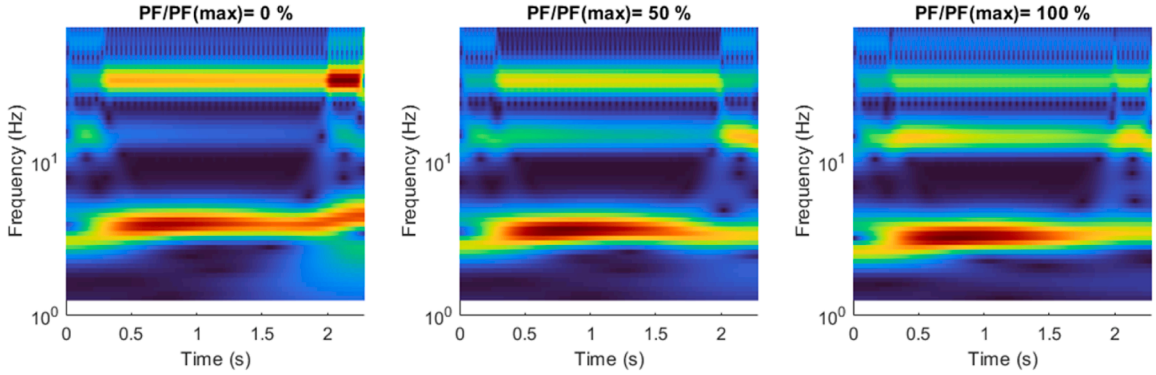

Fig. 5. Time-frequency representations of VBI acceleration responses at 3/8 span of the beam for three PF scenarios.

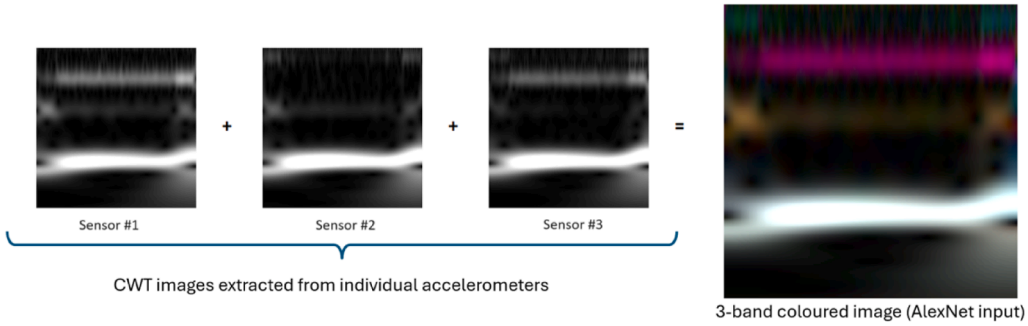

Fig. 6. Composing 3-band colored image by combining CWT data from three sensors.

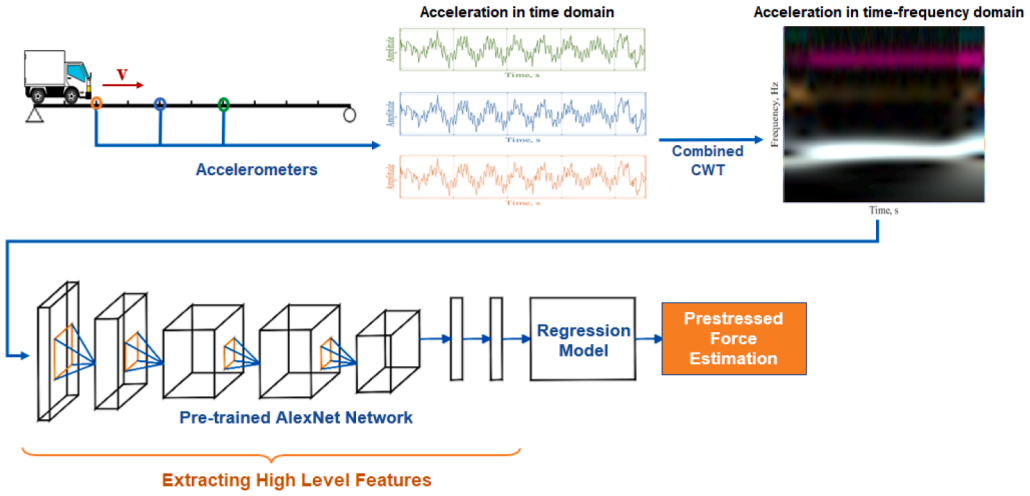

Fig. 7. The flowchart for evaluating the performance of the AlexNet model.

4. A novel hybrid domain adaptation method for pf prediction

4.1. Domain adaptation (DA)

Transfer Learning (TL) is to use the knowledge learned from a source domain to conduct a different task in the target domain. A *Domain* that can be represented as $D = \{X, P(X)\}$ consists of a feature space X and a marginal probability distribution $P(x)$, where $x \in X$. A *Task* that can be represented as $T = \{Y, f(x)\}$ consists of a label set Y and a classifier $f(x)$, and $f(x) = P(y|x)$ is the conditional probability distribution where $y \in Y$.

Assuming a labelled source domain $D_s = \{(x_1, y_1), \ldots, (x_{ns}, y_{ns})\}$ and an unlabelled target domain $D_t = \{x_{ns+1}, \ldots, x_{ns+nt}\}$ with respect to the assumptions that $X_s = X_t$, $Y_s = Y_t$. The idea is that learning a task (source) can facilitate performing a similar task (target) when the source and target domains have certain similarities [26]. The concept can be used for structural health monitoring problems. For example, when the data from an FE model are used to train an ML model, the modelling knowledge can be leveraged for a real bridge despite variations in different structural properties, resulting in a domain shift between the structural health indicator features of the FE model and the real structure.

DA is a technique for transudative TL that seeks to transfer the knowledge of feature representation. With $P_s(x_s) \neq P_t(x_t)$, $P_s(y_s|x_s) \neq P_t(y_t|x_t)$, DA technique aims to learn a feature representation in which the distribution differences are visibly reduced between:

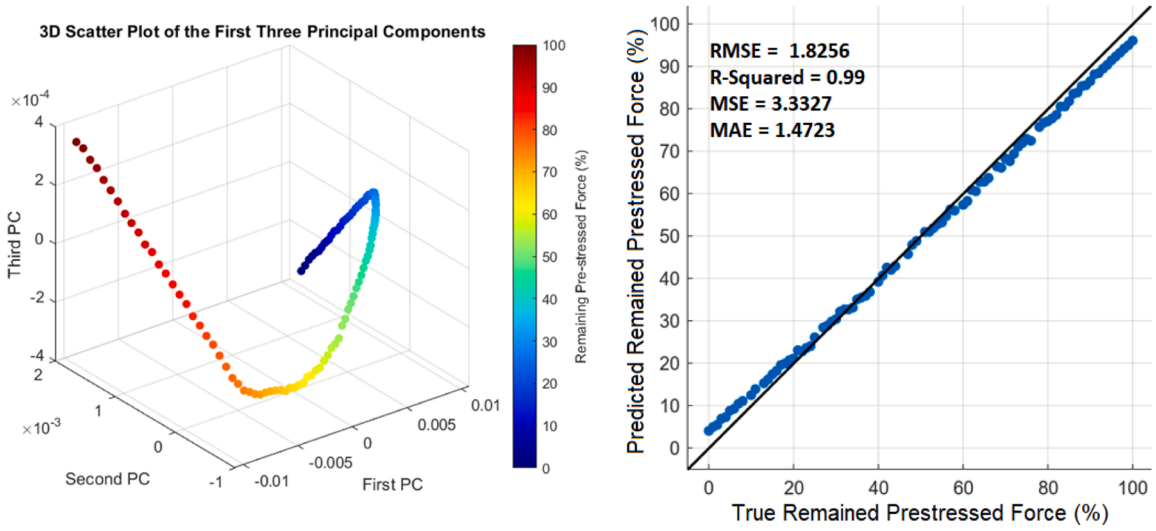

Fig. 8. Feature extraction using AlexNet and correlation of features to PF.

a) marginal distributions: $P_s(x_s)$ and $P_t(x_t)$;
b) class-conditional distributions: $P_s(y_s|x_s)$ and $P_t(y_t|x_t)$.

DA maps the source and target data in a representation feature space by minimizing the differences between their distributions while maintaining the primary structure of the original source and target data [28]. If a regression or classification task can be done in the source feature space, it can also be done in the transformed feature space. In this way, the regression or classification knowledge can be transferred into the target domain and the target unlabelled data can find their own labels [12].

4.2. A novel hybrid DA-based method

Fig. 9 shows the framework of the proposed hybrid DA method. Two DA techniques, e.g. discrepancy-based DA and adversarial-based DA, are synergistically integrated in this study. **Discrepancy-based DA:** In this method, the discrepancy between marginal and conditional distributions is reduced by minimizing the Maximum mean discrepancy (MMD) objective functions [16]. **Adversarial-based DA:** The cross-domain discrepancy is minimized using an adversarial objective function [9]. The original idea was inspired by Goodfellow et al. [11] introducing Generative Adversarial Networks (GAN). In this method, a domain discriminator and a feature extractor are used simultaneously. The domain discriminator is responsible for determining whether input data is related to the source or target domain, and a domain confusion loss is defined for that purpose. The feature extractor is meant to extract features from data to perform a better classification (or regression) and instantaneously deceive the domain discriminator, which means the source and target domain features could not be recognized (i.e. extracting domain-invariant features). In other words, the feature extractor trains to minimize classification (or regression) loss for labelled source samples and maximize the domain confusion loss for all of the samples at the same time [21].

To implant both Maximum Mean Discrepancy (MMD) loss and adversarial loss in a DA-based regression model, three types of loss functions are used:

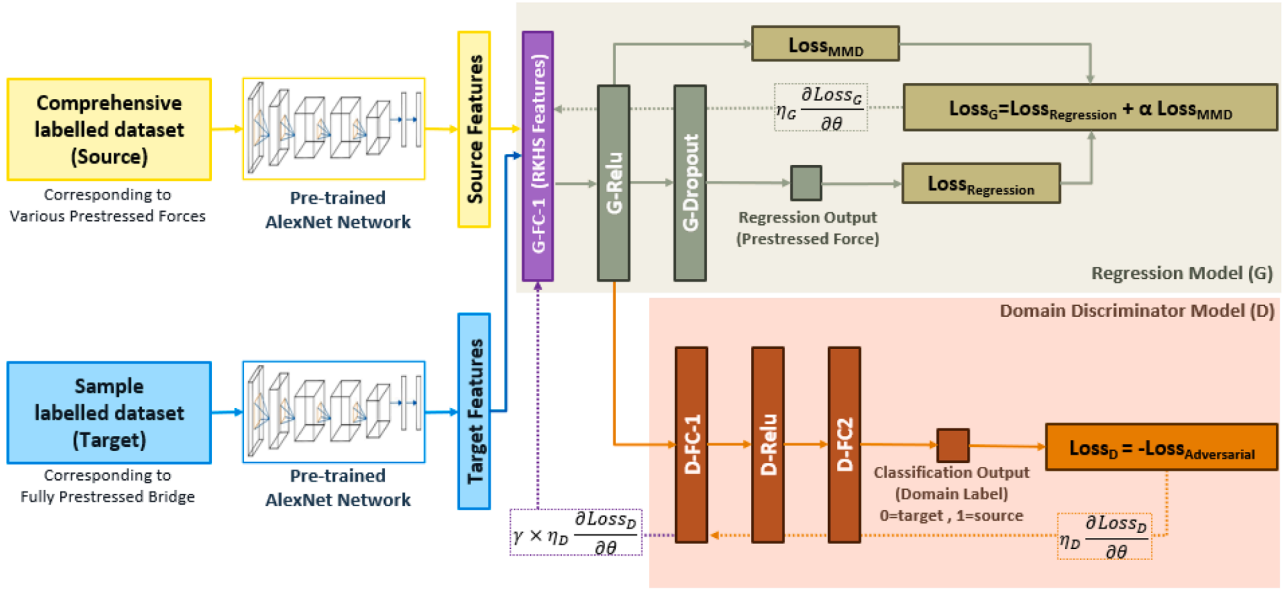

Fig. 9. Framework of the proposed hybrid DA method.

1. *Regression Loss*: is a Mean Squared Error (MSE) loss computed between the predicted PF and the actual force.

$$\text{Loss}_{regression} = mean\left((Y_{predicted} - Y_{actual})^2\right) \tag{14}$$

2. *Maximum Mean Discrepancy (MMD) Loss:* is employed to align the source and target data distributions within a Reproducing Kernel Hilbert Space (RKHS). Its primary aim is to minimize the domain discrepancy for data corresponding to label A, which in our case represents a fully-prestressed bridge with 100 % PF. This label is particularly significant as it is the only label present in the target domain.

$$\text{Loss}_{MMD} = MMD(F_s(X_s|Y_s = A), F_t(X_t|Y_t = A)) \tag{15}$$

where F_s and F_t are feature mapping functions for the source and target domains, respectively. Considering $f_s(x_i)$ as the feature representation of the ith source sample and $f_t(x_j)$ as the feature representation of the jth target sample, the squared MMD loss is calculated as follows:

$$\text{MMD}^2(f_s, f_t) = \frac{1}{n(n-1)} \sum_{\substack{i,j=1 \\ i \neq j}}^{n} k(f_s(x_i), f_s(x_j)) + \frac{1}{m(m-1)} \sum_{\substack{i,j=1 \\ i \neq j}}^{m} k(f_t(x_i), f_t(x_j)) - \frac{2}{n \times m} \sum_{i=1}^{n} \sum_{j=1}^{m} k(f_s(x_i), f_t(x_j)) \tag{16}$$

where n is the number of samples in the source domain, m is the number of samples in the target domain, and $k(x, y)$ is the Gaussian (RBF) kernel function, defined as:

$$k(x, y) = e^{\frac{-||x-y||^2}{2\sigma^2}} \tag{17}$$

where σ is a parameter controlling the width of the kernel.

3. *Adversarial Loss:* aims to make the final feature space domain-insensitive. It contains two parts - discriminator loss for source and target features.

$$\text{Loss}_{Adversarial} = mean(-\log(D(F_s))) + mean(-\log(1 - D(F_t))) \tag{18}$$

where D denotes the discriminator output. Unlike MMD, adversarial loss does not require choosing a kernel or its parameters.

Training processes for the regression model (G) and the discriminator model (D) are integrated into a unified optimization scheme. For network (G), the total loss is a composite of the regression loss and the Maximum Mean Discrepancy (MMD) loss, while the loss function for network (D) is defined as the negative of the adversarial loss:

$$Loss_G = Loss_{Regression} + \alpha Loss_{MMD} \tag{19}$$

$$Loss_D = -Loss_{Adversarial} \tag{20}$$

These two losses can be complementary. While MMD ensures that the source and target distributions are close in an RKHS, adversarial training ensures that a discriminator cannot easily distinguish between the source and target domains. Loss_G is backpropagated through the regression model with a learning rate of η_G, while Loss_D is backpropagated through the discriminator model with a learning rate of η_D. The first fully connected layer is shared between the two models and is updated with a learning rate of $\eta_G + \gamma \times \eta_D$. This shared layer is designed to capture domain-invariant features in RKHS. The optimization process simultaneously minimizes the regression loss, the Maximum Mean Discrepancy (MMD) loss, and maximizes the adversarial loss. This enables the network to learn features that are robust across different domains using a combination of two powerful DA methods.

It should be mentioned that training the hybrid domain adaptation model can be computationally demanding. However, this training process is performed offline. Once the model is trained, the estimation of the prestress force can be performed online in real-time in practice.

5. Evaluation of the proposed method

To evaluate the proposed method, the VBI model described in Section 3.1 is employed to generate the fully labelled source domain dataset. Utilising the proposed hybrid DA technique, PF estimation knowledge is transferred from this fully characterised source domain to a variety of target domains with limited data availability. This section explores how different types of modelling errors and domain shifts affect the hybrid DA model's performance and demonstrates the robustness of the proposed method.

5.1. Training data setup

In the source domain, a dataset of 420 samples is generated for training, including 21 labels representing PF levels ranging from 0 % to 100 % with an interval of 5 %. Each label comprises 20 samples, augmented by introducing a 55 dB SNR white Gaussian noise to the VBI acceleration responses. In the target domain, the only label available in the training dataset is the fully-prestressed condition (Y=100 % PF), as acquiring data for different PF levels of the bridge in real-life scenarios is impractical. For each target domain, 10 samples for 100 % PF label were augmented using a 45 dB SNR white Gaussian noise.

5.2. Model architecture and training process

The model's architecture comprises two fully connected layers for the generator (G) and discriminator (D), initially configured with 50 and 5 neurons, respectively. The training process is governed by a batch size of 16, with learning rates set at 0.5e-3 for the generator (ηG) and 1e-6 for the discriminator (ηD), conducted over 20,000 epochs. For consistency, the model structure is kept similar for training the DA for all the target domains. During this process, domain-invariant features are extracted from PF-sensitive features, resulting in features that are both PF-sensitive and domain-invariant simultaneously.

During the training phase, all labelled source domain data are utilised to compute the regression loss and predict the PF, while the MMD loss and adversarial loss are calculated using data corresponding to the fully-prestressed condition (Y=100 % PF) from both the source and target domains. The loss values over the training process for a sample target are illustrated in Fig. 10.

It is notable that during the training process, where the adversarial loss trends towards negative infinity indicates that the discriminator has become excessively proficient. Under such conditions, the discriminator fails to provide meaningful gradient information for the generator's updates. To counteract this imbalance, a safeguard mechanism is employed: when the discriminator's loss (Loss_D), falls below a threshold of one, its learning rate is linearly reduced to zero. This effectively 'freezes' the discriminator's parameters, preventing further updates and thereby stabilizing the adversarial game. This strategy aims to restore a dynamic balance between the generator and the discriminator, ensuring

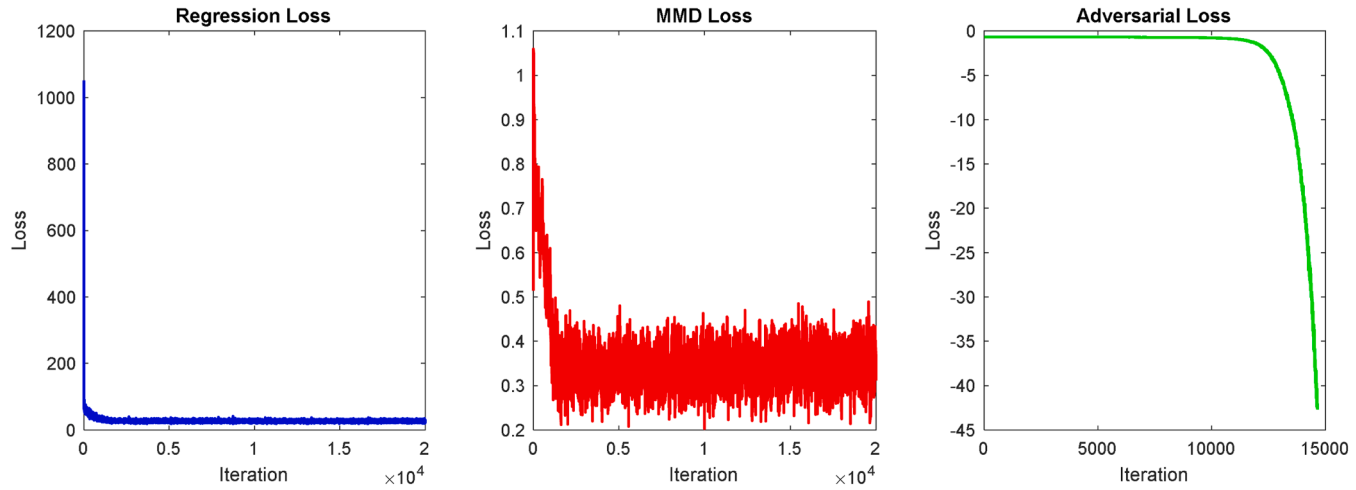

Fig. 10. Evolution of loss values during training the proposed hybrid DA model.

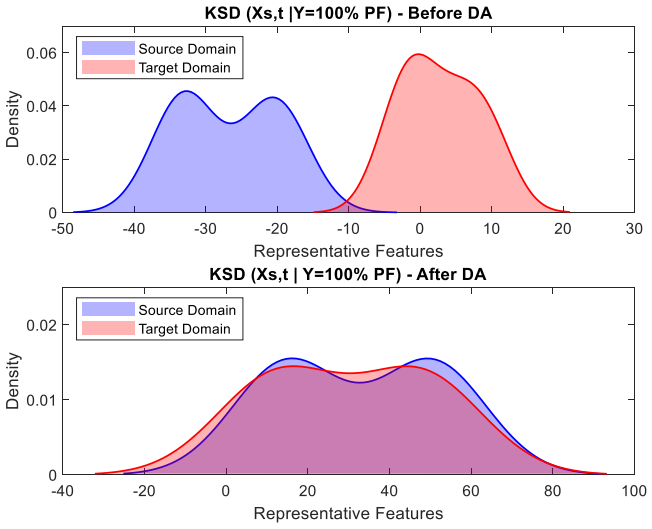

Fig. 11. Feature distribution of source and target domain representative features at 100 % PF condition before and after hybrid DA.

that both can continue to learn effectively.

As a result of optimising the MMD and adversarial loss, the feature distribution discrepancy between the source and target domains is reduced, minimizing the effect of domain shifts in X_t and X_s for the fully-prestressed force condition. The kernelized stein discrepancy (KSD) of the source and target domain representative features corresponding to fully-prestressed condition (Y=100 % PF) before and after DA is presented in Fig. 11.

5.3. Testing and evaluation

In this section, the target domain data for unseen PF conditions (35–95 % PF levels) are studied for testing the performance of the hybrid DA. In this study, the typical values are taken as examples to study the effect of modelling errors on the domain shift and the performance of the proposed hybrid model using different target domains. These target domains are divided into three sub-categories: the bridge and vehicle models, and the road conditions. A detailed breakdown of the target domains is presented in Table 1.

5.3.1. Effect of bridge modelling errors

Modelling discrepancies, including incorrect lengths, variations in

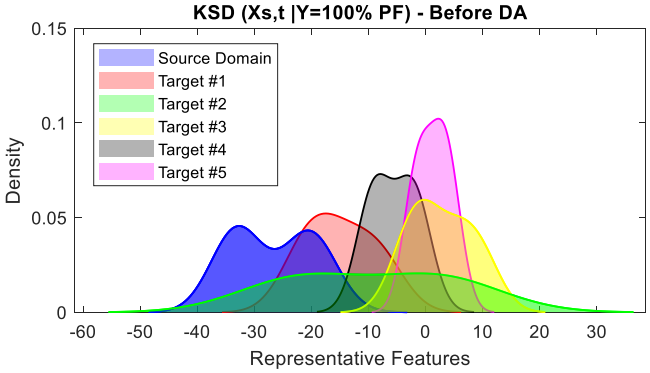

Fig. 12. Feature distribution of target domain representative features for the targets with bridge modelling error at 100 % PF condition.

Table 1
Definition of different target domains for VBI systems.

Category	Parameters	Source Domain	Target Domains								
			Deviations from the Source Domain								
			#1	#2	#3	#4	#5	#6	#7	#8	#9
Bridge	Length	30 m	3 %	-	-	-	-	-	-	-	3 %
	Flexural rigidity (EI)	2.5E+ 10 Nm^2	-	−12 %	-	-	-	-	-	-	−12 %
	Mass for unit length	5000 Kg/m	-	-	−4 %	-	-	-	-	-	−4 %
	Damping ratio (ξ)	0	-	-	-	0.02	-	-	-	-	0.02
	Boundary conditions	P.P.	-	-	-	-	F.P.	-	-	-	F.P.
Road	Roughness class	A	-	-	-	-	-	B			B
Vehicle	Speed	15 m/s	-	-	-	-	-	-	−20 %	-	−20 %
	Parameters	A	-	-	-	-	-	-	-	B	B

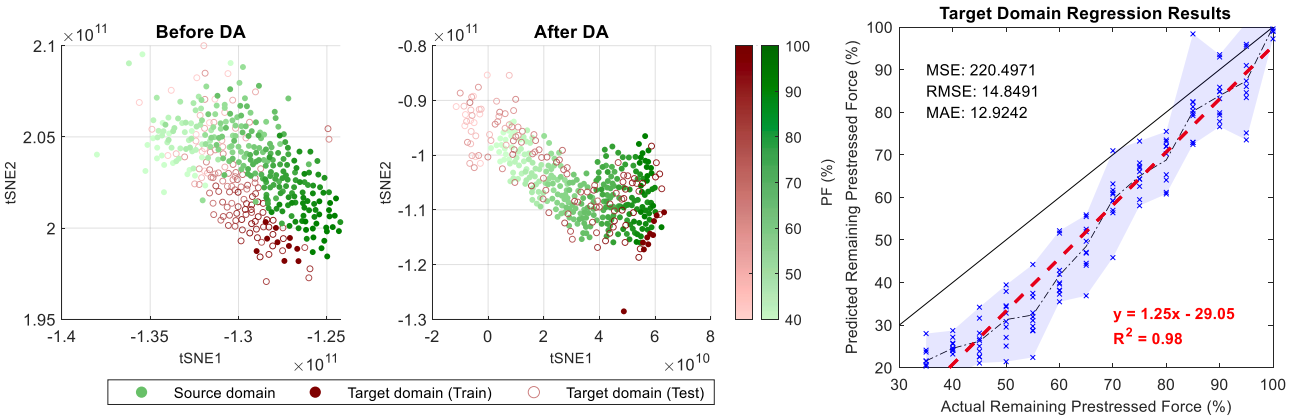

Fig. 13. tSNE analysis of source and target domain features before and after hybrid DA, with PF estimation results for Target 1 (bridge's length modelling error).

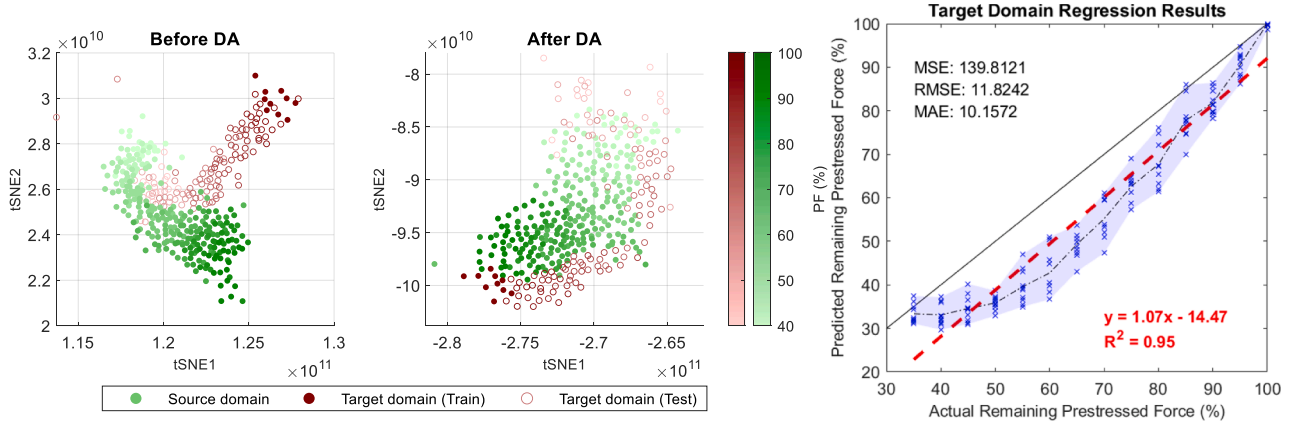

Fig. 14. tSNE analysis of source and target domain features before and after hybrid DA, with PF estimation results for Target 2 (bridge's rigidity modelling error).

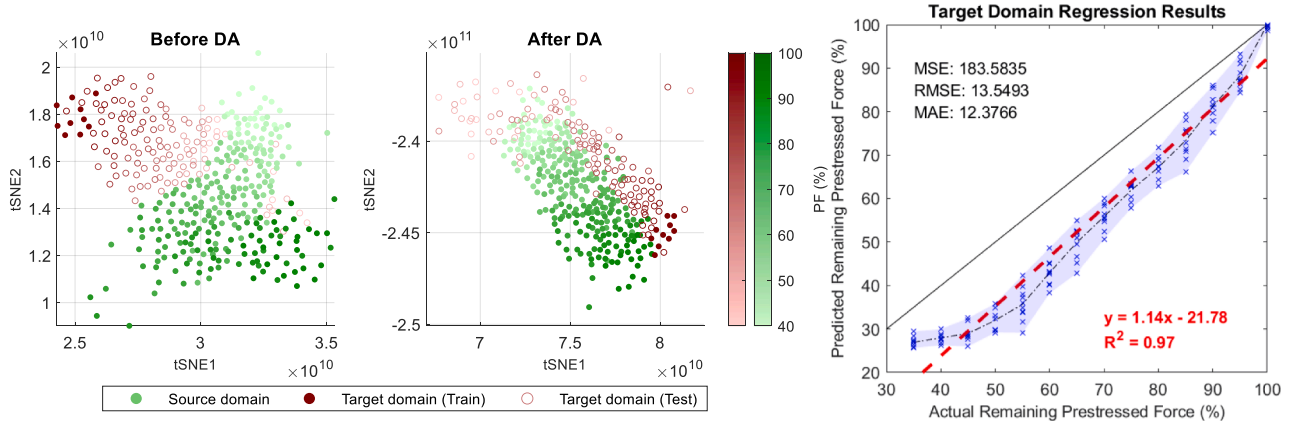

Fig. 15. tSNE analysis of source and target domain features before and after hybrid DA, with PF estimation results for Target 3 (bridge's mass modelling error).

flexural rigidity (EI), mass per unit length and damping ratios, and different boundary conditions, are significant sources of domain shift. These modelling discrepancies correspond to Targets #1-#5 in Table 1. Fig. 12 shows the effect of these variables by illustrating the distribution of representative features for each target. Figs. 13 to 17 show the tSNE representation of the source and target domain features before and after applying hybrid DA for Targets #1-#5, and their PF estimation results for the target domain test data. From the results, a 3 % increase in length (Target #1) results in the minimal domain shift. In contrast, a 0.02 increase in damping ratio (Target #4) and a 4 % decrease in mass (Target #3) induce more substantial shifts. The alteration of boundary conditions from pinned-pinned to fixed-pinned (Target #5) causes a notable domain shift. The most significant effect is observed with a 12 % decrease in EI (Target #2), which dramatically transforms the feature distribution.

5.3.2. *Effect of road surface roughness*

Variations in road surface roughness can notably alter the acceleration responses of the VBI model, impacting both feature extraction and the accuracy of predictions. To evaluate the efficiency of the proposed hybrid DA in adapting to such domain shifts, a target model (Target #6) is set with Class B road roughness, representing increased roughness,

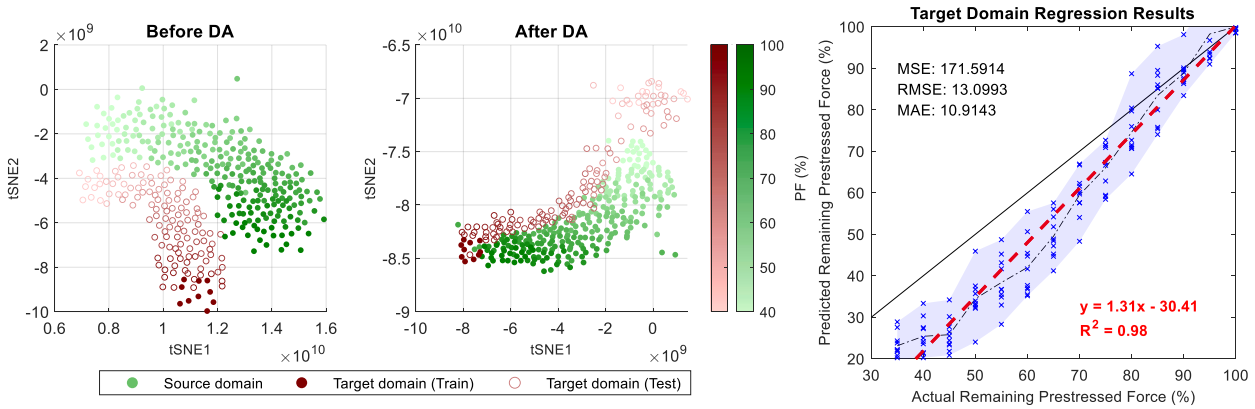

Fig. 16. tSNE analysis of source and target domain features before and after hybrid DA, with PF estimation results for Target 4 (bridge's damping modelling error).

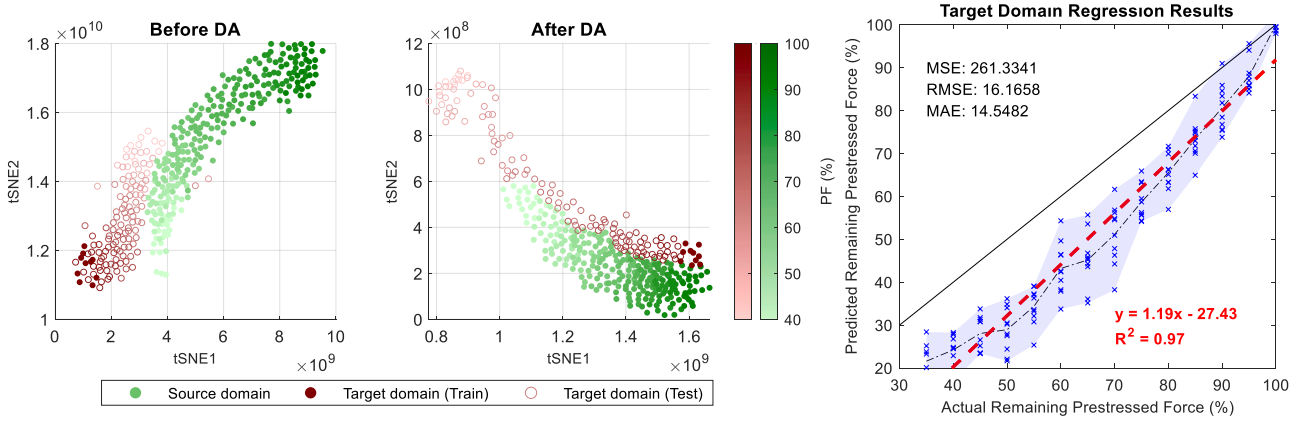

Fig. 17. tSNE analysis of source and target domain features before and after hybrid DA, with PF estimation results for Target 5 (bridge's boundary conditions modelling error).

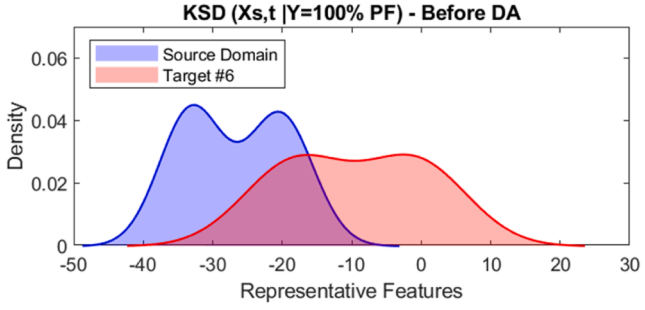

Fig. 18. Feature distribution of target domain representative features for the target with road roughness modelling error at 100 % PF condition.

whereas the source model featured Class A road roughness. Fig. 18 depicts the effects of surface roughness on domain shift by demonstrating the distribution of representative features for the source and target domains. There is a clear shift in the feature space.

Fig. 19 shows the tSNE visualization of source and target domain features by the proposed hybrid approach and the predicted prestressed forces. The results show that the domain feature shift caused by road surface roughness is reduced by the proposed hybrid model. There is an approximate linear relationship between the predicted and actual prestressed forces.

5.3.3. *Effect of errors in vehicle parameters and speed*

Variations in vehicle parameters and speed significantly impact the dynamic interaction between the vehicle and the bridge, influencing PF-sensitive features and PF estimation results. Target 7 involves reducing vehicle speed from 15 m/s to 12 m/s, while Target 8 entails switching from Vehicle A to Vehicle B. Vehicle A's parameters are as listed in Section 3.1, with natural frequencies of 1.63, 2.30, 10.35, and 15.10 Hz. For Vehicle B, both mass and spring stiffness are increased by 20 %, resulting in natural frequencies of 1.78, 2.11, 10.35, and 15.10 Hz. Fig. 20 illustrates the effect of modelling errors in vehicle parameters and speed on domain shift by displaying the distribution of representative features for the source and each referenced target domain. It is evident that these errors induce more significant domain shifts than those typically observed in scenarios involving bridge modelling errors.

Figs. 21 and 22 depict the efficiency of the hybrid DA approach in mitigating domain shifts attributed to variations in road vehicle speed and modelling inaccuracies. Additionally, these figures provide PF estimation results for the target domain test data, demonstrating the approach's capability in scenarios where discrepancies exist between the speed or parameters of the modelled and actual passing vehicle, ensuring reliable prestress force predictions.

Since the discrepancy between the finite element model of the bridge and the actual bridge is not precisely determined in reality, any of the aforementioned targets could occur. Evaluation results demonstrate that the proposed hybrid DA approach effectively minimizes domain shifts in all scenarios, enabling PF estimation to be performed within an acceptable error range, which generally leans towards conservative estimates. Further analysis of this approach is presented in the following section, where the impact of a multi-variational target, the selection of hyperparameters, and the method's ability to handle unseen domains

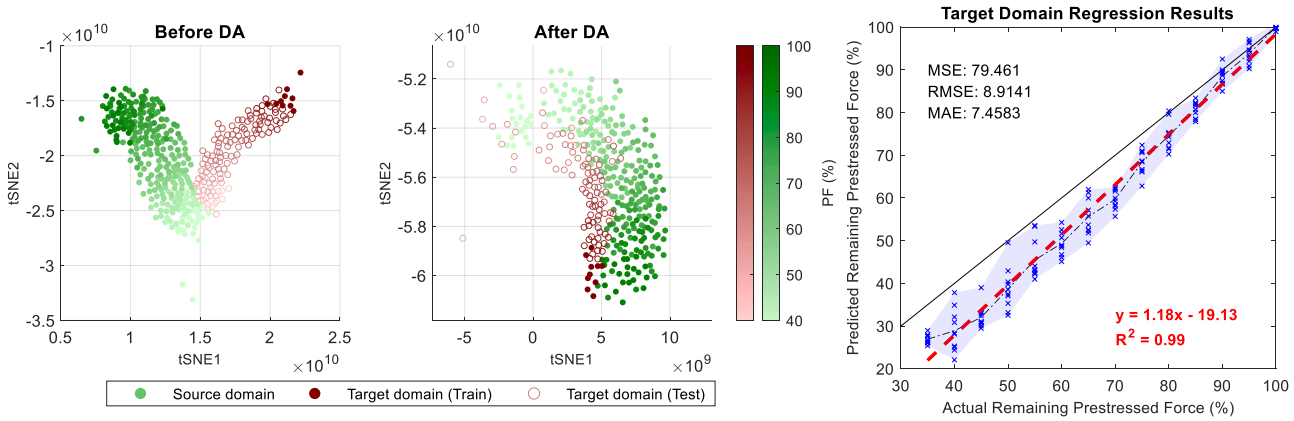

Fig. 19. tSNE analysis of source and target domain features before and after hybrid DA, with PF estimation results for Target 6 (road roughness modelling error).

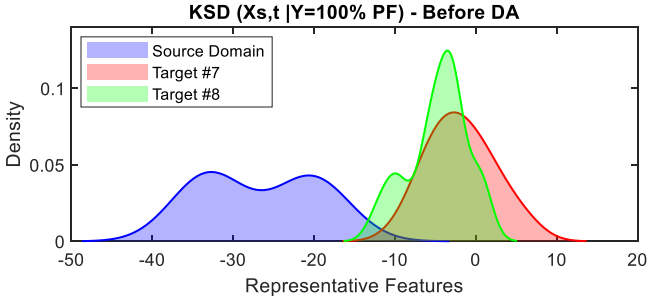

Fig. 20. Feature distribution of target domain representative features for the target with vehicle modelling error at 100 % PF condition.

are examined.

5.4. Further explorations on a target with multiple deviations

A target model was set up to incorporate all the specified deviations, presenting a scenario with modelling errors in the bridge, road, and vehicle simultaneously. This target was particularly important as it combined multiple sources of discrepancies, testing the model's ultimate capability in domain adaptation. Fig. 23 illustrates the domain shift between this target domain and the source domain by showing the distribution of their representative features at 100 % PF condition.

Fig. 24 highlights the capabilities of the hybrid DA technique in adjusting to significant variations between source and target domains. tSNE representation of the source and target domains illustrates changes in feature distributions before and after the application of hybrid DA. The PF estimation outcomes for test data in the target domain confirm the method's resilience and efficacy, even in the face of significant domain shifts, showing its practical applicability.

5.4.1. Network hyperparameters study

In this section, the effect of hyperparameter variations on the model's performance is investigated through a series of tests, with each hyperparameter being modified individually. Adjustments were made to the number of neurons in both the generator and discriminator layers, batch size, learning rates, number of epochs, MMD kernel size, the ratio of MMD loss to regression loss, and the adversarial loss factor. Table 2 presents a comparison, showing the impact of each hyperparameter adjustment on the performance of the model in transferring PF estimation knowledge from the source to Target 9.

These results show that a proper selection of the hyperparameters can effectively increase the performance of the Hybrid DA approach. Reducing the batch size and the learning rate of the regression model (Generator G) improves PF identification performance, suggesting that a finer update during training increases the model's ability to learn and generalize from the data. A substantial reduction in the number of neurons in Generator G's hidden layers (from 50 to 20) leads to improved performance, indicating that the model can achieve optimal performance with a relatively simpler architecture. This could imply that the features extracted from the pre-trained CNN are robust and the regression model does not require excessive complexity to capture the underlying patterns, thereby promoting a more efficient and less overfitting-prone model structure.

In opposition, reducing the number of neurons in the Discriminator D's hidden layers (from 5 to 3) tends to deteriorate the model's performance, as reflected by increased MAE and MSE. This suggests that the

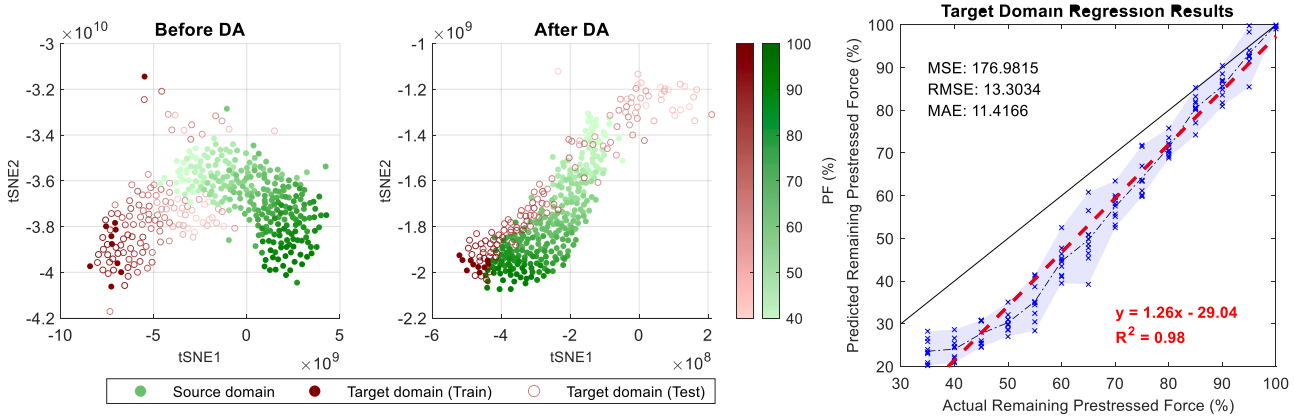

Fig. 21. tSNE analysis of source and target domain features before and after hybrid DA, with PF estimation results for Target 7 (vehicle speed error).

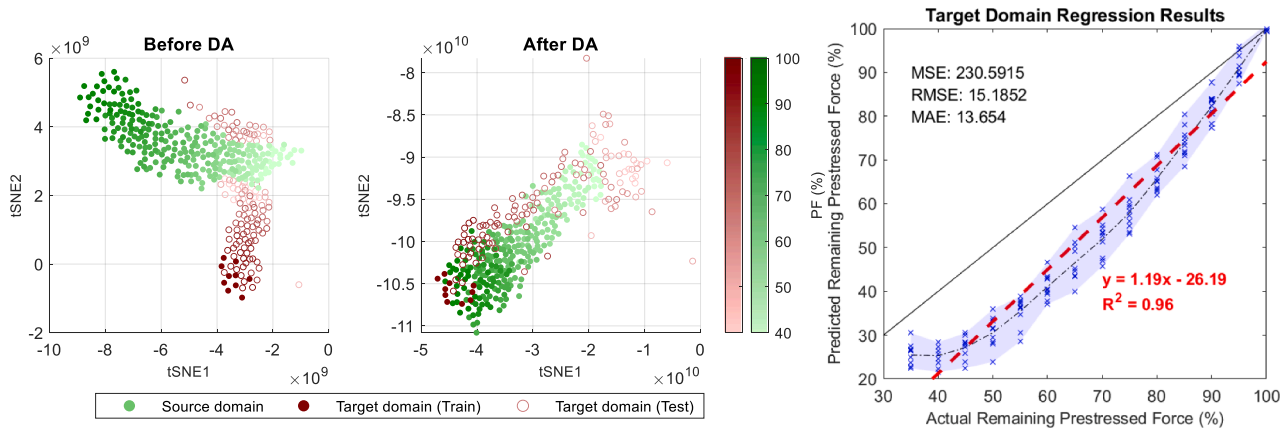

Fig. 22. tSNE analysis of source and target domain features before and after hybrid DA, with PF estimation results for Target 8 (vehicle modelling error).

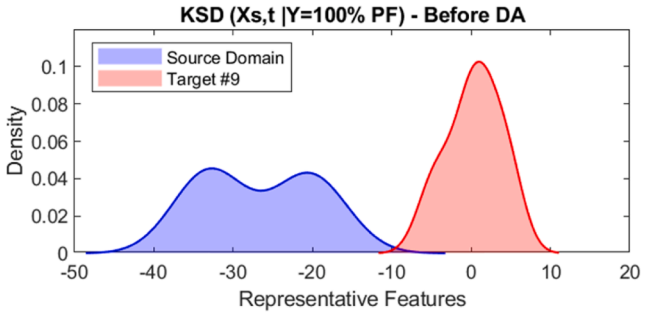

Fig. 23. Feature distribution of target domain representative features for the target with multiple deviations at 100 % PF condition.

Discriminator D may require a certain level of complexity to effectively distinguish between the source and target domain features, and effectively play its role in the adversarial component of the training. Reducing the number of epochs to half (from 20,000 to 10,000) shows an increase of the MAE from 12.72 to 15.02, signifying that the model benefits from extended training periods due to the complexity of the domain adaptation task.

In terms of the MMD kernel size (σ), the study suggests that a smaller kernel size yields better performance in aligning the distributions of the source and target domain features. Moreover, adjusting the MMD to regression loss ratio (α) from 1000 to 100 results in a noticeable improvement in performance, indicating the importance of balancing the domain adaptation component (MMD loss) with the task-specific component (regression loss) in the final loss function of the generator.

While the adversarial loss factor (γ) does not show high sensitivity to changes, its optimal adjustment maintains a harmonious adversarial training process, ensuring that the feature extractor and the discriminator are well-aligned in their objectives.

Based on this parameter study, the model was trained on the target 9 datasets with 20 neurons in network G, 5 neurons in network D, a batch size of 16, a learning rate of 1e-4 for G, a learning rate of 1e-6 for D, 20,000 epochs, an MMD kernel size of 5, an MMD/Reg. Loss ratio of 1000, and an Adversarial Loss Factor of 100. The final regression results, presented in Fig. 25, demonstrate a notable improvement in network performance. The MAE was reduced from 12.72 to 9.28, and the RMSE was reduced from 15.72 to 10.71.

5.4.2. *Evaluating model robustness across unseen domains*

The proposed method is designed to leverage the data from a single label of the target domain to adapt the source and target domains for the PF estimation task. This is a practical method to utilise a limited set of available data from a desired domain. This approach relies on having the structural VBI response in the bridge's fully prestressed state and assumes that other bridge factors remain relatively stable, in the event of a loss in prestressed force. However, real-world scenarios can be more complex; structural properties of bridges change over time, potentially leading to variations in VBI responses. Moreover, damages to bridges may not solely pertain to PF loss. For instance, local stiffness reductions due to cracks can alter how a bridge reacts to the passing vehicle. Additionally, the vehicle parameters and speed during the testing phase may vary from those employed in the domain adaptation process.

This section investigates the impact of such unseen domains on the effectiveness of the proposed method. The hybrid DA model is trained using data from "Target 9", wherein Vehicle B crosses the bridge at a

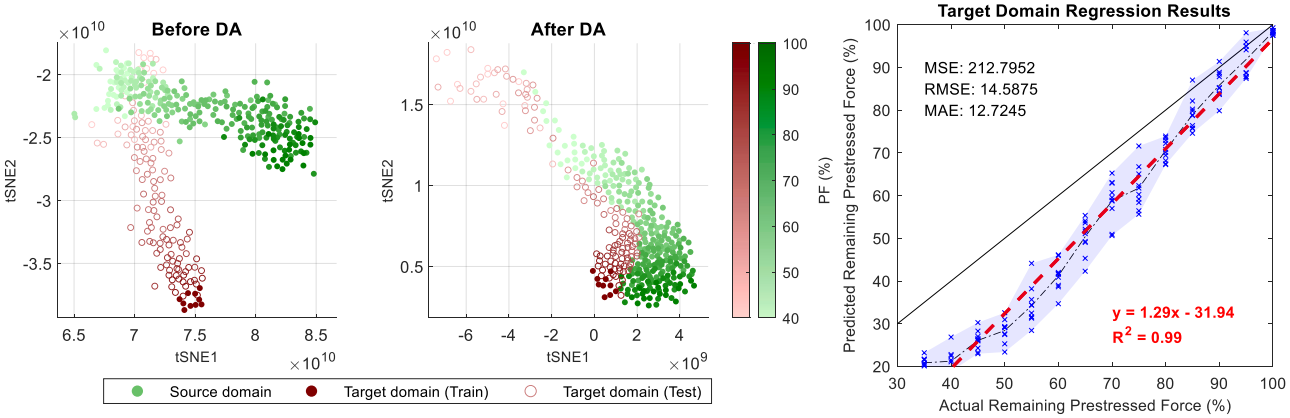

Fig. 24. tSNE analysis of source and target domain features before and after hybrid DA, with PF estimation results for Target 9 (multiple deviations).

Table 2
Model Hyperparameters Studies.

		MAE	RMSE
Benchmark model		12.72	14.59
Comparison models			
Hyperparameter	Modifications		
No. of Neurons for G	50–20	9.82	11.88
No. of Neurons for D	5–3	13.99	15.72
Batch Size	16–32	14.76	17.07
Learning Rate G (η_G)	0.5e−3–1e−4	10.88	12.66
Learning RateD (η_D)	1e−6–0.5e−6	12.77	14.69
No. of Epochs	20,000–10,000	15.02	16.48
MMD kernel size (σ)	5–10	13.07	15.09
MMD/Reg. Loss ratio (α)	1000–100	11.09	12.9
Adv. Loss Factor (γ)	100–10	12.98	15.07

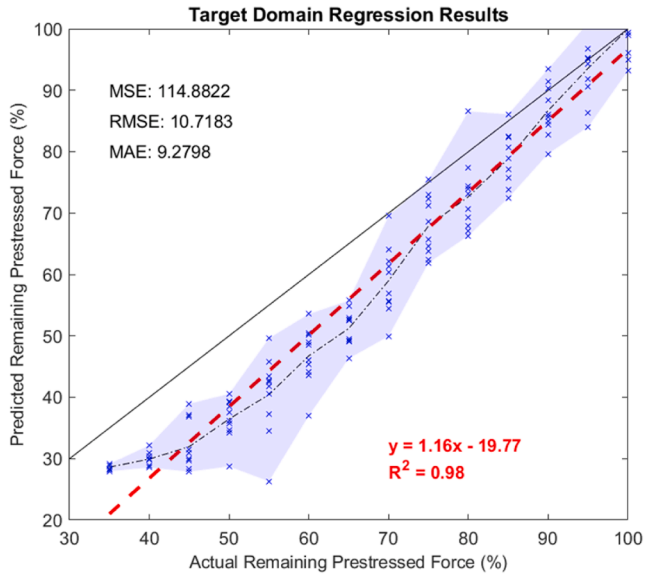

Fig. 25. Regression Results for Target 9 with Carefully Selected Hyperparameters.

speed of 12 m/s, with the bridge's total mass assumed to be 4800 kg. To assess the model's robustness, four unseen domains are introduced for evaluation: two related to changes in bridge parameters and two concerning vehicle parameters and speed.

The first unseen domain aims to assess the model's performance in the presence of cracks, utilising the Wahab et al. [33] model for crack introduction. A crack with a severity (γ) of 20 %, a length (β) of 0.2 in the damaged zone, and a variation in Young's modulus (n) set to 2, affects one-quarter of the bridge's length. The regression outcomes for this domain are depicted in Fig. 26(a). The second unseen domain explores the model's response to a reduction in the bridge's mass to 4600 kg, with corresponding regression results shown in Fig. 26(b). The third domain considers variations in the passing vehicle's parameters, slightly altered from Vehicle B, with natural frequencies of 1.70, 2.22, 10.35, and 15.10 Hz. The outcomes for this domain are illustrated in Fig. 26(c). Finally, in the fourth domain, the vehicle speed is adjusted to 8 m/s, with results presented in Fig. 26(d).

These evaluations reveal that the model's performance experiences a slight decline across unseen domains, which are likely encountered during a bridge's lifespan testing. Nonetheless, the outcomes remain sufficiently reliable, underscoring the proposed method's robustness in addressing unseen domains. This adaptability highlights the method's potential for practical application in monitoring and maintaining bridge safety.

6. Discussions

This section discusses the effectiveness and limitations of the proposed hybrid domain adaptation approach for prestressed force estimation in bridges:

- This approach demonstrates the feasibility of transferring finite element model knowledge to real-world applications, closing the simulation-to-reality gap.
- The hybrid domain adaptation approach successfully mitigates domain shifts caused by variations in bridge parameters, vehicle characteristics, and road surface conditions. Results show a significant reduction in MAE from 37.14 to 9.28 and RMSE from 46.40 to 10.71 before and after domain adaptation for Target 9. Reducing the batch size, adjusting the learning rates, and simplifying the generator architecture further enhanced performance, with a reduction in MAE from 12.72 to 9.28 and RMSE from 15.72 to 10.71 for the most challenging target domain (Target 9).
- The method effectively handled unseen domain shifts, such as a 20 % reduction in vehicle speed, a 12 % decrease in bridge rigidity, and variations in road surface roughness, with MAE remaining below 15 for all the unseen domains.
- Despite the demonstrated effectiveness of the hybrid domain adaptation approach, certain constraints remain. For instance, the method requires baseline responses from the structure in its fully prestressed state, which requires initiating monitoring at an early stage. The proposed hybrid model could be updated continuously through continuing learning from continuing monitoring data. Additionally, while the model adapts well to various domain shifts, highly complex or rapidly shifting real-world conditions may still be challenging. Future work includes extending the approach to a broader range of bridge types and performing comprehensive experimental validations under diverse modelling uncertainties and environmental factors.

7. Conclusions

In this study, a novel Hybrid Domain Adaptation (Hybrid DA) approach has been proposed for the prediction of the remaining prestressed force in bridge structures to address the highly challenging issues of limited labelled data in real-world scenarios and discrepancies between simulations and actual structures. The method innovatively uses a single label in the target domain to mitigate the domain shift. The PF identification regression model is trained on AlexNet features extracted from the time-frequency responses of a finite element model of the Vehicle-Bridge Interaction (VBI) system. A second finite element model, chosen as the target domain, acknowledges common discrepancies between synthetic and real-world data. The Hybrid DA strategy, which integrates Maximum Mean Discrepancy (MMD) and adversarial learning, aligns features from both domains, creating a unified feature space for accurate PF prediction in the target domain. This approach makes a significant contribution to the field of structural health monitoring and bridge condition assessment. The following conclusions are obtained,

1) The results show that the proposed hybrid DA model could be reliable and efficient in predicting the prestressed force from the VBI responses.
2) The proposed approach could reduce the domain shift due to the uncertainty caused by the modelling errors of the VBI system with only the fully-prestressed label.
3) In practice, there are datasets from limited damage scenarios. The proposed approach could be used to predict the prestressed forces for unseen datasets.
4) While this research represents a significant leap in structural health monitoring, the complexities of real-world applications necessitate

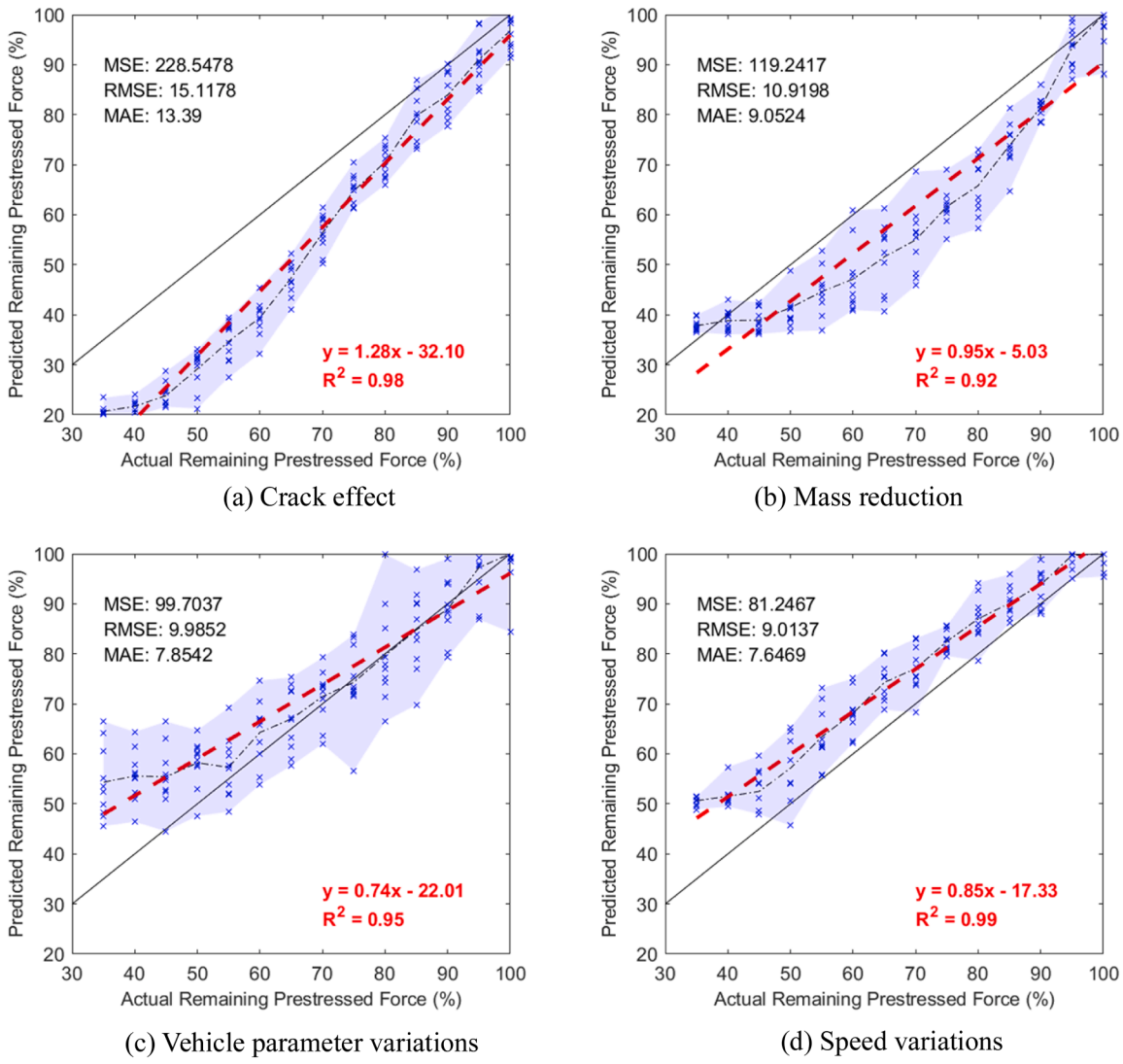

Fig. 26. Model performance evaluation across unseen domains.

further experimental validations to ensure the robustness, adaptability, and overall reliability of the proposed method under diverse conditions.

CRediT authorship contribution statement

Zhu Xinqun: Writing – review & editing, Supervision, Resources, Project administration, Funding acquisition. **Li Jianchun:** Writing – review & editing, Supervision. **Yu Yang:** Writing – review & editing. **Chan Tommy H.T.:** Writing – review & editing, Supervision, Funding acquisition. **Talaei Saeid:** Writing – original draft, Visualization, Validation, Methodology, Investigation, Formal analysis, Data curation, Conceptualization.

Declaration of Competing Interest

The authors declare that they have no known competing financial interests or personal relationships that could have appeared to influence the work reported in this paper.

Acknowledgment

Authors would like to acknowledge the support from Australian Research Council (ARC) grant DP220102045 and the first author also likes to acknowledge the financial support of UTS Doctoral Scholarship (UTSD) and the Research Training Program (RTP), which greatly contributed to the completion of this research.

Data availability

Data will be made available on request.

References

[1] Avci O, Abdeljaber O, Kiranyaz S, Hussein M, Gabbouj M, Inman DJ. A review of vibration-based damage detection in civil structures: from traditional methods to machine learning and deep learning applications. Mech Syst Signal Process 2021; 147:107077.
[2] Azimi M, Pekcan G. Structural health monitoring using extremely compressed data through deep learning. Comput-Aided Civ Infrastruct Eng 2020;35(6):597–614. https://doi.org/10.1111/mice.12517.
[3] Balafas K, Kiremidjian AS. Development and validation of a novel earthquake damage estimation scheme based on the continuous wavelet transform of input and output acceleration measurements. Earthq Eng Struct Dyn 2015;44(4):501–22.
[4] Bonopera M, Chang K-C. Novel method for identifying residual prestress force in simply supported concrete girder-bridges. Adv Struct Eng 2021;24(14):3238–51.
[5] Bonopera M, Chang K-C, Lee Z-K. State-of-the-art review on determining prestress losses in prestressed concrete girders. Appl Sci 2020;10(20):7257.
[6] Breccolotti M. On the evaluation of prestress loss in PRC beams by means of dynamic techniques. Int J Concr Struct Mater 2018;12(1):1.
[7] Chan TH, Yung T. A theoretical study of force identification using prestressed concrete bridges. Eng Struct 2000;22(11):1529–37.

[8] Farahani A, Voghoei S, Rasheed K, Arabnia HR. A brief review of domain adaptation. Adv Data Sci Inf Eng 2021:877–94.
[9] Ganin Y, Lempitsky V. Unsupervised domain adaptation by backpropagation. Int Conf Mach Learn 2015.
[10] Gardner P, Bull LA, Gosliga J, Dervilis N, Worden K. Foundations of population-based SHM, Part III: heterogeneous populations - mapping and transfer (Article) Mech Syst Signal Process 2021;149:107142. https://doi.org/10.1016/j.ymssp.2020.107142.
[11] Goodfellow I, Pouget-Abadie J, Mirza M, Xu B, Warde-Farley D, Ozair S, Courville A, Bengio Y. Generative adversarial nets. Adv Neural Inf Process Syst 2014:27.
[12] Guan H, Liu M. Domain adaptation for medical image analysis: a survey. IEEE Trans Biomed Eng 2021;69(3):1173–85.
[13] Ho D-D, Kim J-T, Stubbs N, Park W-S. Prestress-force estimation in PSC girder using modal parameters and system identification. Adv Struct Eng 2012;15(6):997–1012.
[14] Kim J-T, Yun C-B, Ryu Y-S, Cho H-M. Identification of prestress-loss in PSC beams using modal information. Struct Eng Mech 2004;17(3-4):467–82.
[15] Krizhevsky A, Sutskever I, Hinton GE. ImageNet classification with deep convolutional neural networks. Commun Acm 2017;60(6):84–90. https://doi.org/10.1145/3065386.
[16] Kumagai A, Iwata T. Unsupervised domain adaptation by matching distributions based on the maximum mean discrepancy via unilateral transformations. Proc AAAI Conf Artif Intell 2019.
[17] Law, S., Wu, S., & Shi, Z. (2008). Moving load and prestress identification using wavelet-based method.
[18] Law SS, Zhu XQ. Dynamic behavior of damaged concrete bridge structures under moving vehicular loads. Eng Struct 2004;26(9):1279–93.
[19] Law SS, Zhu XQ. Moving loads-dynamic analysis and identification techniques introduction. Struct Infrastruct Book Ser 2011;8:1–24. https://doi.org/10.1201/b10561.
[20] Li H, Lv Z, Liu J. Assessment of prestress force in bridges using structural dynamic responses under moving vehicles. Math Probl Eng 2013;2013.
[21] Li J, Li Z, Lü S. Feature concatenation for adversarial domain adaptation. Expert Syst Appl 2021;169:114490.
[22] Lu Z, Law S. Identification of prestress force from measured structural responses. Mech Syst Signal Process 2006;20(8):2186–99.
[23] Mulcahy NL. Bridge response with tractor-trailer vehicle loading. Earthq Eng Struct Dyn 1983;11(5):649–65.
[24] Nguyen T-T, Phan TTV, Ho D-D, Pradhan AMS, Huynh T-C. Deep learning-based autonomous damage-sensitive feature extraction for impedance-based prestress monitoring. Eng Struct 2022;259:114172.
[25] Normung I.O. f(1995). . International Organization for Standardization, ISO.⟨https://books.google.com.au/books?id=1kyioAEACAAJ⟩. ISO 8608: Mechanical Vibration, Road Surface Profiles, Reporting of Measured Data: International Standard.
[26] Pan SJ, Yang QA. A survey on transfer learning. Ieee Trans Knowl Data Eng 2010;22(10):1345–59. https://doi.org/10.1109/tkde.2009.191.
[27] Poole J, Gardner P, Dervilis N, Bull L, Worden K. On statistic alignment for domain adaptation in structural health monitoring. Struct Health Monit- Int J 2022. https://doi.org/10.1177/14759217221110441.
[28] Rashidi S., Tennakoon R., Rekavandi A.M., Jessadatavornwong P., Freis A., Huff G., Easton M., Mouritz A., Hoseinnezhad R., Bab-Hadiashar A.(2022). It-ruda: Information theory assisted robust unsupervised domain adaptation.arXiv preprint arXiv:2210.12947..
[29] Silik A, Noori M, Altabey WA, Ghiasi R, Wu Z. Comparative analysis of wavelet transform for time-frequency analysis and transient localization in structural health monitoring. Struct Durab Health Monit 2021;15(1):1.
[30] Talaei, S., Zhu, X., Li, J., Yu, Y., & Chan, T.H. (2023). Transfer learning based bridge damage detection: Leveraging time-frequency features. Structures,
[31] Tang Q, Xin J, Jiang Y, Zhou J, Li S, Chen Z. Novel identification technique of moving loads using the random response power spectral density and deep transfer learning. Measurement 2022;195:111120.
[32] Thedy J, Liao K-W, Tseng C-C, Liu C-M. Bridge health monitoring via displacement reconstruction-based NB-IoT technology. Appl Sci 2020;10(24):8878.
[33] Wahab MA, De Roeck G, Peeters B. Parameterization of damage in reinforced concrete structures using model updating. J Sound Vib 1999;228(4):717–30.
[34] Wu G-M, Yi T-H, Yang D-H, Li H-N. Damage detection of tension pendulums in cable-stayed bridges using structural frequency variance. J Perform Constr Facil 2021;35(1):04020126.
[35] Xiang Z, Chan TH, Thambiratnam DP, Nguyen A. Prestress and excitation force identification in a prestressed concrete box-girder bridge. Comput Concr 2017;20:617–25.
[36] Yang S, Huang Y. Damage identification method of prestressed concrete beam bridge based on convolutional neural network. Neural Comput Appl 2021;33:535–45.
[37] Yi T-H, Yao X-J, Qu C-X, Li H-N. Clustering number determination for sparse component analysis during output-only modal identification. J Eng Mech 2019;145(1):04018122.
[38] Zhu XQ, Law SS. Damage detection in simply supported concrete bridge structure under moving vehicular loads. J Vib Acoust 2006;129(1):58–65. https://doi.org/10.1115/1.2202150.